

# The cold rain-on-snow event of June 2013 in the Canadian Rockies — characteristics and diagnosis

John W. Pomeroy,<sup>1\*</sup> Xing Fang<sup>1</sup> and Danny G. Marks<sup>2</sup>

<sup>1</sup> Centre for Hydrology, University of Saskatchewan, Saskatoon, Canada

<sup>2</sup> USDA Agricultural Research Service, Northwest Watershed Research Center, Boise, USA

## Abstract:

The June 2013 flood in the Canadian Rockies featured rain-on-snow (ROS) runoff generation at alpine elevations that contributed to the high streamflows observed during the event. Such a mid-summer ROS event has not been diagnosed in detail, and a diagnosis may help to understand future high discharge-producing hydrometeorological events in mountainous cold regions. The alpine hydrology of the flood was simulated using a physically based model created with the modular cold regions hydrological modelling platform. The event was distinctive in that, although at first, relatively warm rain fell onto existing snowdrifts inducing ROS melt; the rainfall turned to snowfall as the air mass cooled and so increased snowcover and snowpacks in alpine regions, which then melted rapidly from ground heat fluxes in the latter part of the event. Melt rates of existing snowpacks were substantially lower during the ROS than during the relatively sunny periods preceding and following the event as a result of low wind speeds, cloud cover and cool temperatures. However, at the basin scale, melt volumes increased during the event as a result of increased snowcover from the fresh snowfall and consequent large ground heat contributions to melt energy, causing snowmelt to enhance rainfall–runoff by one fifth. Flow pathways also shifted during the event from relatively slow sub-surface flow prior to the flood to an even contribution from sub-surface and fast overland flow during and immediately after the event. This early summer, high precipitation ROS event was distinctive for the impact of decreased solar irradiance in suppressing melt rates, the contribution of ground heat flux to basin scale snowmelt after precipitation turned to snowfall, the transition from slow sub-surface to fast overland flow runoff as the sub-surface storage saturated and streamflow volumes that exceeded precipitation. These distinctions show that summer, mountain ROS events should be considered quite distinct from winter ROS and can be important contributors to catastrophic events. Copyright © 2016 John Wiley & Sons, Ltd.

KEY WORDS rain-on-snow; flooding; snowmelt; flowpaths; cold regions hydrological model; Canadian Rockies

Received 22 October 2015; Accepted 29 April 2016

## INTRODUCTION

Over 3 days in late June 2013, 250 mm of precipitation fell on the partially snow-covered and heavily instrumented Marmot Creek Research Basin, Canadian Rockies, contributing to the largest recorded flood in the region, the destruction of most gauging stations in the research basin and the most expensive natural disaster in Canadian history (Pomeroy *et al.*, 2016). The event hydrometeorology has been described in detail by Liu *et al.* (2016), the historical hydrological context of this flood described by Whitfield and Pomeroy (2016) and the impact of antecedent conditions examined by Fang and Pomeroy (2016); these papers and the overview by Pomeroy *et al.* (2016) all suggest that snowmelt, including rain-on-snow (ROS), was an important contributor to the flood in addition to heavy rainfall.

The remarkable celerity and synchrony of translation of precipitation into river discharge was noted by Pomeroy *et al.* (2016). However, the magnitude and processes governing snowmelt and ROS contributions to runoff in this event, or to other late-spring and early-summer ROS events in alpine regions around the world, have not been investigated in detail.

Rain-on-snow events occur when rain falls on a snowpack and are common in maritime mountain snowpacks such as in the US Pacific Northwest (Harr, 1981; Marks *et al.*, 1998, 2001; McCabe *et al.*, 2007; Mazurkiewicz *et al.*, 2008; Wayand *et al.*, 2015) and also occur in eastern North America (Pradhanang *et al.*, 2013; Buttle *et al.*, 2016), central Europe (Singh *et al.*, 1997; Sui and Koehler, 2001; Garvelmann *et al.*, 2015), northern Eurasia (Ye *et al.*, 2008) and the Himalayas (Singh and Kumar, 1997). They have recently started occurring in the Canadian Prairies as the region responds to climate change (Dumanski *et al.*, 2015; Stadnyk *et al.*, 2016). When relatively warm rainfall occurs, it has been observed that melt rates can be

\*Correspondence to: John W. Pomeroy, Centre for Hydrology, University of Saskatchewan, Saskatoon, Canada.  
E-mail: john.pomeroy@usask.ca

enhanced, which may cause flooding (Harr, 1981; Sui and Koehler, 2001). The enhanced snowmelt rates during ROS are not entirely a result of advected energy carried by rainfall but have substantial contributions from turbulent sensible and latent heat transfer associated with saturated conditions and air and dew point temperatures above 0 °C (Marks *et al.*, 1998, 2001). Flooding in ROS events is a result of combined contributions of snowmelt water, condensation and rainfall and is not necessarily exclusively a result of enhanced snowmelt rates (Mazurkiewicz *et al.*, 2008; Wayand *et al.*, 2015). The long duration of snowpacks at high elevations in mountains, including into the summer season, makes these particularly prone to ROS.

Temperate zone snow models that rely on empirical temperature index or related techniques have great difficulty in cold mountain regions (Swanson, 1998) and in general, temperature index-type models do not perform well because of their lack of physical basis (Walter *et al.*, 2005). The Cold Regions Hydrological Modelling platform (CRHM) (Pomeroy *et al.*, 2007) is a flexible, modular modelling system that offers a comprehensive range of processes of importance in alpine regions such as the Canadian Rockies (e.g. blowing snow, interception and sublimation of snow, energy balance snowmelt, slope radiation, canopy influence on radiation, canopy gap effect on snow). It has been demonstrated by Clark *et al.* (2015a, b) that flexible, modular modelling systems with a strong physical basis have great utility in assessing structural uncertainty in hydrological models and selecting the most appropriate algorithms in models, thereby reducing uncertainty in predictions.

The objective of this paper is to describe the June 2013 alpine ROS event in Marmot Creek Research Basin and diagnose the energy and mass balance processes controlling runoff formation in this high-elevation catchment using a physically based model. The paper will attempt to determine to what degree snowmelt from alpine regions contributed to this flood event. Did the ROS enhance or dampen the ongoing summer snowmelt? What were the sources of energy for the ROS event, and how did they differ from fair-weather summer snowmelt? What were the flow pathways controlling the rapid runoff rates for this event, and how did they differ from those slower pathways operating in non-flood conditions?

## METHODS

### *Study site and field observations*

The study was conducted in the upper elevations of Marmot Creek Research Basin (MCRB) (50°57'N, 115°09'W) in the Kananaskis Valley, Alberta, Canada, located

in the Front Ranges of the Canadian Rocky Mountains (Figure 1; Fang and Pomeroy, 2016). Elevation ranges from 1590 m.a.s.l at the Marmot Creek outlet to 2829 m.a.s.l at the summit of Mount Allan. Exposed rock surface and talus are present in the high alpine part of basin (1956 to 2829 m.a.s.l); alpine larch (*Larix lyallii*) and short shrub are present around the treeline at approximately 2016 to 2379 m.a.s.l. The surficial soils are primarily poorly developed mountain soils consisted of glaciofluvial, till surficial and postglacial colluvium deposits (Beke, 1969). Relatively impermeable bedrock is found at the higher elevations and headwater areas (Jeffrey, 1965). Annual precipitation is about 1100 mm at the higher elevations, of which approximately 70 to 75% occur as snowfall, with the percentage increasing with elevation (Storr, 1967). The mean monthly air temperature over the basin ranges from 14 °C in July to −10 °C in January.

Meteorological observations of air temperature, relative humidity, wind speed, precipitation, soil temperature and incoming short-wave radiation were collected from the Centennial Ridge and Fisera Ridge hydrometeorological stations (Figure 1; DeBeer and Pomeroy, 2010; Ellis *et al.*, 2010; MacDonald *et al.*, 2010). Precipitation was measured with an Alter-shielded Geonor weighing precipitation gauge and a Hydrological Services tipping bucket rain gauge at Fisera Ridge; the Alter shield was corrected for wind-induced undercatch of snowfall. Meteorological data were spatially distributed across the upper basin with adjustments for temperature by a constant environmental lapse rate (0.75 °C/100 m) and adjustments for precipitation based on seasonal gradients from several years of observations at multiple elevations. Vapour pressure was conserved for unsaturated conditions and not allowed to exceed saturation vapour pressure when extrapolated. Radiation inputs were adjusted for slope and sky view using the methods described by Fang *et al.* (2013). Snow surveys were conducted over the winter and spring from transects established near the meteorological stations. Measurements of streamflow were conducted at the outlet of the 1.2 km<sup>2</sup> Upper Marmot Creek Basin (UMCB) shown in DeBeer and Pomeroy (2010). More details of field observations are provided by Fang *et al.* (2013).

### *Model*

The CRHM (Pomeroy *et al.*, 2007) was used to develop hydrological models for UMCB and Fisera South-face. CRHM is an object-oriented, modular and flexible platform for assembling physically based hydrological models. With CRHM, the user constructs a purpose-built model or 'project' from a selection of possible basin spatial configurations, spatial resolutions

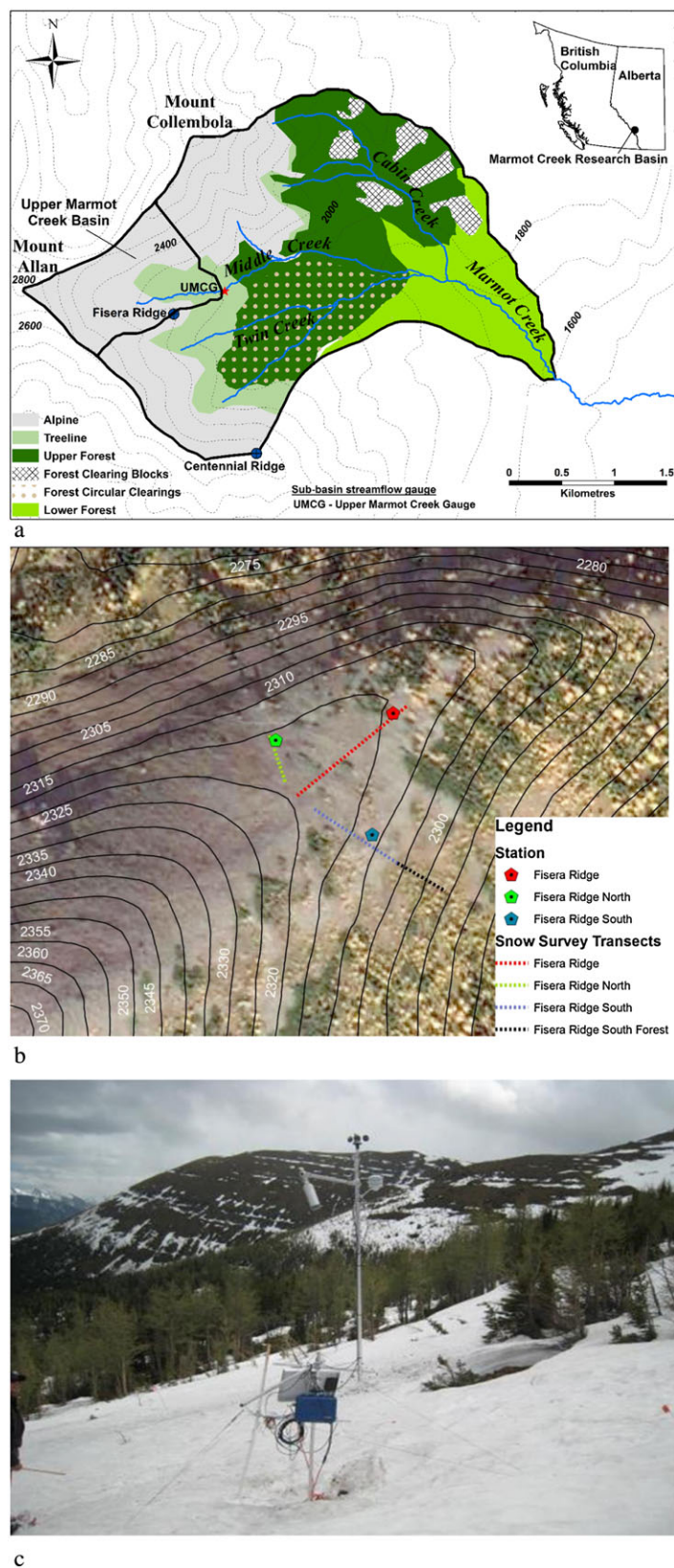


Figure 1. Marmot Creek Research Basin showing (a) location of Upper Marmot Creek Basin (UMCB), elevations, forest cover, streamflow gauge and the location of Fisera Ridge and Centennial Ridge meteorological stations; (b) detailed aerial image of Fisera Ridge showing three meteorological stations and snow survey transects; (c) view of Fisera South-face late June snowpack

and physical process modules of varying degrees of physical complexity. Basin discretization is performed via dynamic networks of hydrological response units (HRUs), whose number and nature are selected based on the variability of basin attributes and the level of physical complexity chosen for the project. Physical complexity is selected by the user in light of hydrological understanding, parameter availability, basin complexity, meteorological data availability and the objective flux or state for prediction. The process algorithms available in CRHM have been extensively field tested in mountains (Pomeroy *et al.*, 2012; Fang *et al.*, 2013; Rasouli *et al.*, 2015). CRHM includes algorithms rarely found in hydrological models such as those for calculating shortwave radiation through forest canopies on slopes (Ellis and Pomeroy, 2007), longwave radiation from partly cloudy skies and mountain terrain (Sicart *et al.*, 2006), enhanced longwave emissions from canopies (Pomeroy *et al.*, 2009), precipitation phase using psychrometric principles (Harder and Pomeroy, 2014), snow surface temperature (Ellis *et al.*, 2010), canopy gap radiative transfer, forest canopy snow interception,

sublimation, drip and unloading (Ellis *et al.*, 2010, 2011, 2013), alpine blowing snow transport and sublimation (MacDonald *et al.*, 2010) and alpine snowmelt and snowmelt runoff (DeBeer and Pomeroy, 2010).

CRHM was used to assemble a set of physically based modules into hydrological model to simulate the dominant hydrological processes found in MCRB. The model created is similar to that described by Fang and Pomeroy (2016) and is shown in Figure 2, with boxes signifying process modules described in the succeeding texts and arrows denoting fluxes of energy and mass. Critical to initial conditions is the redistribution of snow by wind to form late lying snowdrifts by the prairie blowing snow model (MacDonald *et al.*, 2010). For ROS and rainfall-runoff analysis, relevant process calculations include precipitation phase using the psychrometric energy balance model (Harder and Pomeroy, 2013) and snowmelt using the Snobal snowmelt model (Marks *et al.*, 1998). The psychrometric energy balance precipitation phase model calculates turbulent transfer to a falling hydrometeor and then its temperature presuming thermodynamic equilibrium at the ice-bulb or wet-bulb

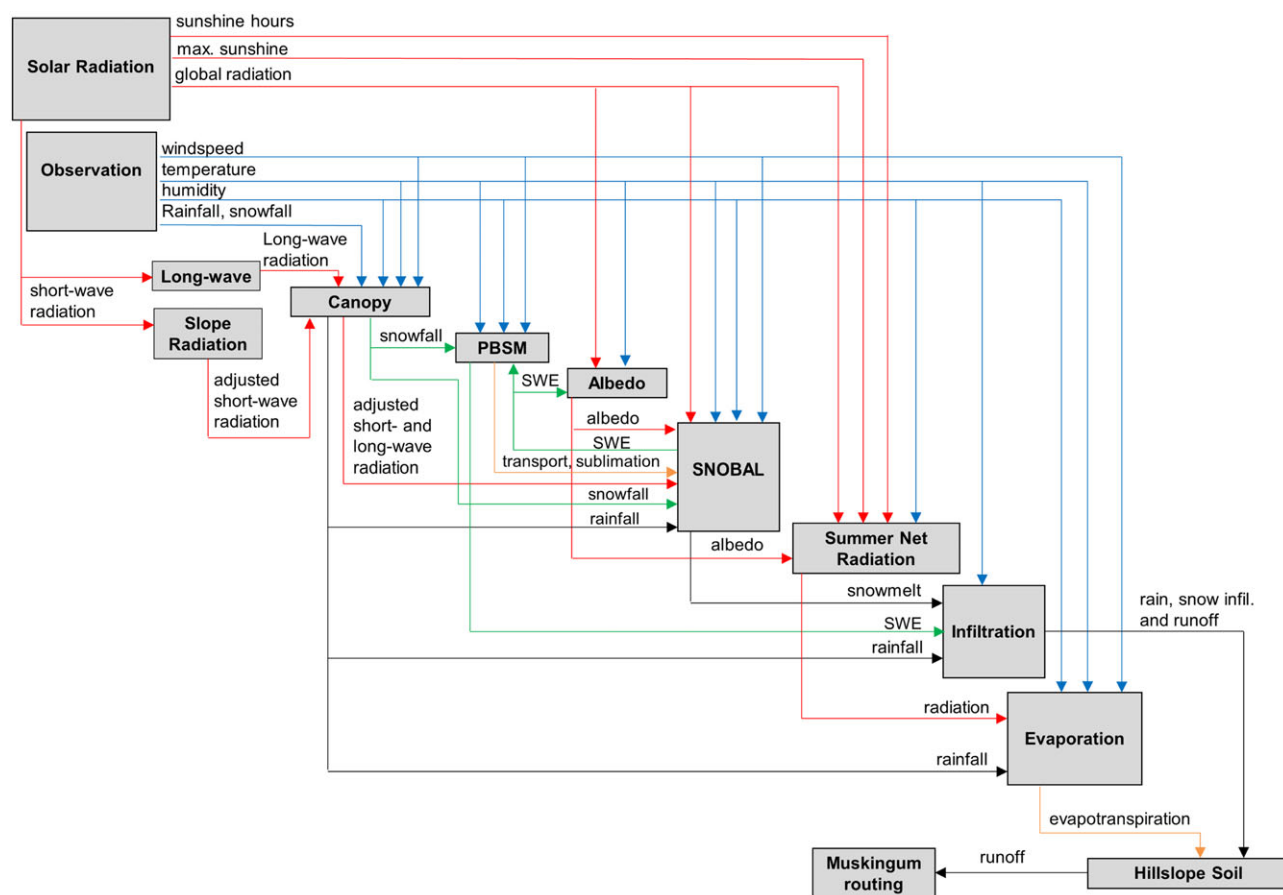


Figure 2. Module structure of cold regions hydrological model set up for Upper Marmot Creek showing process and data modules and flow of variables dealing with radiation (red line), meteorology (blue line), evaporation and sublimation (orange line), snow (green line) and water (black line)

temperature and an adjustment for typical deviations from equilibrium conditions – its advantage is that there are no parameters that require calibration as is common in hydrological model precipitation phase estimation and so uncertainty is reduced (Harder and Pomeroy, 2014). Snobal (SNOBAL in Figure 2) is a coupled one-dimensional energy and mass budget model for a two-layer snowpack. It diagnoses snow layer temperature based on a balance of net radiation, sensible and latent heat flux to the upper layer and conduction between layers as shown in Figure 3. The lower layer energy balance is also affected by conductive heat flow with the ground. Snobal includes sublimation and condensation associated with latent turbulent heat fluxes and route rainfall through the snowpack, permitting energy exchange of heat advected from rain to the snowpack. CRHM also has modules (Canopy, Longwave, Slope Radiation) that calculate short- and long-wave radiation to Snobal in complex terrain and under forest canopies (Ellis *et al.*, 2010), wind speed variation over complex terrain (Walmsley *et al.*, 1989) and snow redistribution by wind (Prairie Blowing Snow Model) (Pomeroy and Li, 2000) and through the forest canopy (Ellis *et al.*, 2010), including sublimation losses from blowing and intercepted snow. Modules for flood and antecedent conditions include the evaporation, hillslope soil and Muskingum routing modules. Routing uses Muskingum and 'lag and route' methods as described by Fang *et al.* (2013). Updates for the evapotranspiration calculation (evaporation) to a Penman–Monteith resistance formulation from the Granger–Gray approach described by Fang *et al.* (2013) are detailed by Fang and Pomeroy (2016).

There are reports of remarkable flow celerity during the 2013 flood (Pomeroy *et al.*, 2016). To ensure that this

aspect of runoff is modelled correctly, the CRHM version run for this analysis includes a modification of the hillslope module comprising a near-surface detention layer over two soil layers and a groundwater layer with provision for depressional storage and macropore flow between sub-surface layers and from surface to groundwater (Figure 4). The detention layer is a new interface between the soil and atmospheric processes and allows the surface runoff to flow through a porous medium as a transient flow pathway. It was incorporated to address temporary snow damming (Fang *et al.*, 2013) and water storage in loose organic material in the alpine tundra (Beke, 1969) and forest floor (Keith *et al.*, 2010). During detention, the volume of surface runoff over an event is not affected, but the runoff rate is controlled by the detention layer, whose drainage factors are calculated as follows:

$$Dts_{\text{organic\_K}} = cK_{s\_organic} \left( \frac{Dts}{Dts_{\text{max}}} \right)^{(3+2/\lambda_{org})} \tan(\theta) \frac{Dts_{\text{max}}}{1000} \quad (1)$$

where  $Dts_{\text{organic\_K}}$  ( $\text{mm day}^{-1}$ ) is the drainage factor for lateral flow in detention layer during snow-free period, and  $K_{s\_organic}$  is the saturated hydraulic conductivity for the organic material and was set to  $1.1 \times 10^{-4} \text{ m s}^{-1}$  based on the averaged value measured by Keith *et al.* (2010).  $Dts$  (mm) and  $Dts_{\text{max}}$  (mm) are the storage of water and water storage capacity in the detention layer respectively.  $Dts_{\text{max}}$  was set as 50 mm for alpine and 100 mm for non-alpine part of basin; these values are similar to the observations by Keith *et al.* (2010).  $\lambda_{org}$  (dimensionless) is the pore size distribution index for the organic material and was set to 3 from the value recommended by Brooks

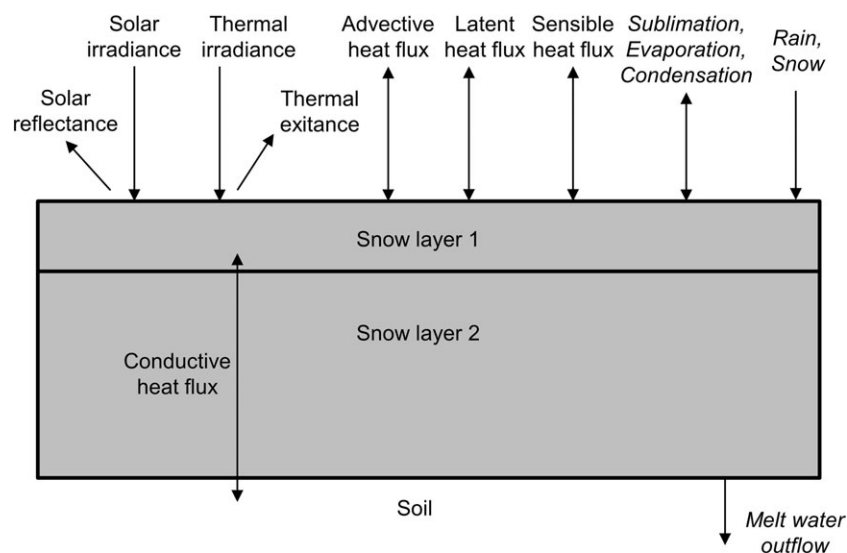


Figure 3. Snobal layering and energy and mass flux configuration



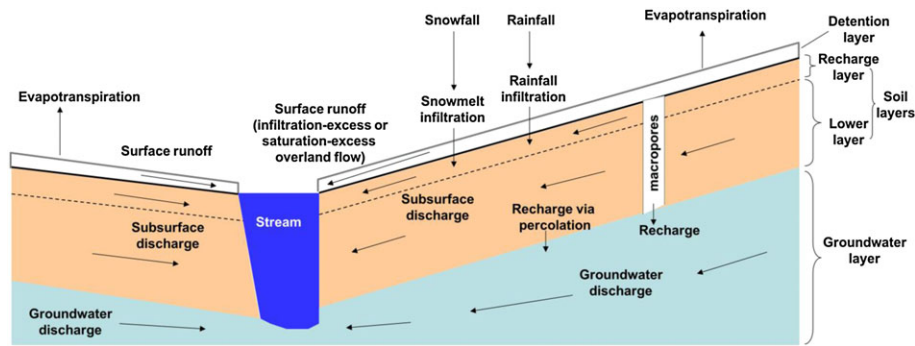


Figure 4. Conceptual representation of the CRHM hillslope module with control volumes for detention layer, two soil layers, groundwater layers and surface depressions or macropores and their interactions. Note that saturated porous media flow always occurs in the groundwater layer and can episodically occur in the detention and soil layers

and Corey (1966).  $\theta$  (radian) is the ground slope, and  $c$  (dimensionless) is a unit conversion factor from  $\text{m s}^{-1}$  to  $\text{mm day}^{-1}$  equal to  $86.4 \times 10^6$ . Derivation of equation 1 is outlined by Fang *et al.* (2013) using Darcy's law along with Brooks and Corey (1964) relationship.

During the snow-covered period, the drainage factor for lateral flow in the detention layer  $Dts_{\text{snow\_K}}$  ( $\text{mm day}^{-1}$ ) is estimated based on formulation of Darcy's law by Colbeck (1972, 1975) and relationships among water pressure, saturation and permeability:

$$Dts_{\text{snow\_K}} = cK_{s\_snow} \left( \frac{Dts}{Dts_{\text{max}}} \right)^{S_I} \sin(\theta) \frac{Dts_{\text{max}}}{1000} \quad (2)$$

$S_I$  (dimensionless), the soil index or pore size distribution index in the permeability of snow and water saturation relationship (Wankiewicz, 1979) was set as 4.8, the mean for metamorphosed snow (McGurk and Kattelman, 1986).  $K_{s\_snow}$  ( $\text{m s}^{-1}$ ) is the saturated hydraulic conductivity of snow and is calculated using empirical relation by Shimizu (1970):

$$K_{s\_snow} = \left[ 0.077 \left( \frac{d_g}{1000} \right)^2 \exp \left( -7.8 \frac{\rho_d}{\rho_w} \right) \right] \left( \frac{\rho_w g}{\mu_w} \right) \quad (3)$$

where  $d_g$  (mm) is the grain size,  $\rho_d$  and  $\rho_w$  are the density of snow ( $\text{kg m}^{-3}$ ) and water ( $1000 \text{ kg m}^{-3}$ ),  $g$  is the gravitational acceleration (taken as  $9.8 \text{ m s}^{-2}$ ), and  $\mu_w$  is the dynamic viscosity of water (taken as  $0.001787 \text{ kg m}^{-1} \text{ s}^{-1}$ ).

The model spatial representation was set up for UMCB using a distributed HRU structure focussing on slope, aspect, soils, hillslope location and forest cover. This was based on a Lidar-derived digital elevation model (Hopkinson *et al.*, 2012), soil surveys (Beke, 1969), forest inventory maps and drainage delineation using ArcGIS (Pomeroy *et al.*, 2012). The five HRUs chosen for the basin are alpine forest north-facing, alpine forest south-facing, alpine talus north-facing, alpine talus

south-facing and valley bottom meadow; their spatial configuration is shown in Figure 5. The valley bottom meadow HRU corresponds to the Upper Marmot Creek stream and adjacent floodplain and valley bottom. The main parameters for slope, aspect, elevation, soil layers depth, leaf area index, vegetation height and HRU area in UMCB are shown in Table I.

A similar CRHM single HRU model was also created for the Fisera South-face snowpack that had been simulated as part of a larger model for MCRB (Fang and Pomeroy, 2016). The Fisera South-face HRU results show detailed energy and mass balances for an open site, with a pre-existing snowpack as a residual from over-winter snowdrift formation. Important parameters for this site are its slope ( $18^\circ$ ), aspect ( $95^\circ$ ), vegetation height (0.92 m) and density ( $0.6 \text{ shrubs m}^{-2}$ ).

## RESULTS

### Meteorological and snow observations

The regional and local meteorological and hydrological conditions during the flood are described in detail by Pomeroy *et al.* (2016), Liu *et al.* (2016) and Fang and Pomeroy (2016). At MCRB, similar depths of precipitation fell at all elevations measured (1436 to 2325 m), with measurements of 251 mm from 19–25 June 2013. This measurement was compromised because the event started as rainfall and shifted to snowfall on 21–22 June. The Geonor weighing precipitation gauge overtopped on 21 June and could not be accessed for maintenance because of flood damages to trails and roads at lower elevations. During the snowfall from 21–22 June, the depth of fresh snow on the ground was used to estimate precipitation, assuming a World Meteorological Organisation standard assumption of a fresh snow depth of  $100 \text{ kg m}^{-3}$  for temperate conditions. Given the shallow depth of fresh snow on the ground, the additional uncertainty in the mass balance of the event from this density assumption is

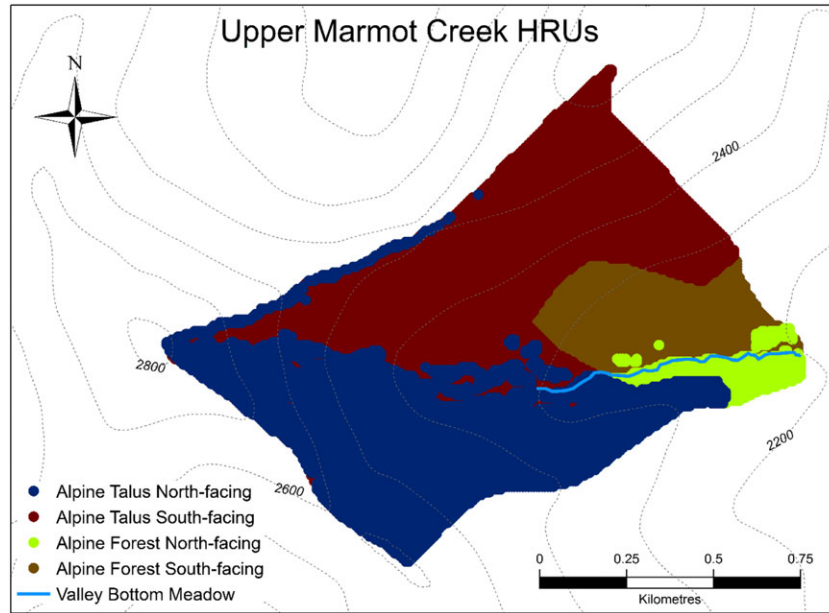


Figure 5. Hydrological response units in Upper Marmot Creek Basin

Table I. Upper Marmot Creek Basin parameters

HRU name	Area (km <sup>2</sup> )	Elevation (m.a.s.l)	Aspect (°)	Slope (°)	Maximum organic layer depth (mm)	Soil layer storage capacity (mm)	Winter leaf area index	Vegetation height (m)
Alpine Talus North-facing	0.44	2468	75	30	50	250	0	0.14
Alpine Talus South-facing	0.52	2458	147	26	50	250	0	0.14
Alpine Forest South-facing	0.17	2278	141	18	100	550	1.1	3
Alpine Forest North-facing	0.04	2233	45	18	100	550	1.1	3
Valley Bottom Meadow	0.008	2242	102	10	100	1000	0	0.14

Total basin area is 1.178 km<sup>2</sup>.

also small. Air temperatures were 13 °C just before the event and as high as 8 °C during rainfall on the 19th, dropping to 0.4 °C during snowfall on the 21st (Figure 6A). The atmosphere became saturated on the 18th and remained saturated through the 21st (Figure 6B). Wind speeds were variable, rising from near-calm conditions on the 18th to a peak of 4 m s<sup>-1</sup> on the 20th and then dropping with an average of 2 m s<sup>-1</sup> with a peak of 5.5 m s<sup>-1</sup> during the precipitation event (Figure 6C). Fisera Ridge meteorological station was snow-free at the beginning of the precipitation event but developed an 8 cm deep snowpack on the 21st which ablated after the 22nd (Figure 6E). At the Fisera South-face meteorological station, there was a snowpack of about 0.65 m depth at the beginning of the event early on the 19th which had ablated to 0.49 m depth by the end of the 20th and then accumulated snow reaching 0.63 m later on the 21st (Figure 6F). Heavy rain caused the ultrasonic sensor to fail during much of the 19th and 20th (Figure 6D and F). Rainfall and snowfall rates during the event remained less

than 12 mm h<sup>-1</sup> and only exceeded 6 mm h<sup>-1</sup> on the 19th and 20th, with daily totals rising from 39 mm on the 19th to 111 mm on the 20th, and then falling to 75 and 18 mm on the 21st and 22nd respectively. Snowfall totalled at least 10 mm water equivalent and occurred from 0830 to 1630 h on the 21st but was likely underestimated by snow-depth measurements because it was mixed with rain, and some melted as it reached the ground.

Snow surveys were conducted along Fisera Ridge on a 15-point transect running from treeline forest to open tundra and along the Fisera South-face on a 29-point transect from open tundra into treeline forest on the early afternoons of 13 and 26 June 2013. Snow-covered area fraction on Fisera Ridge dropped from 0.53 to 0.27 and on the Fisera South-face from 0.97 to 0.55 over the interval. Snowpack on the Fisera Ridge and Fisera South-face transects ablated over 13 days by 83 and 218 mm snow water equivalent (SWE) from 182 and 353 mm SWE on the 13th respectively. The average ablation for forested sites that remained snow covered on Fisera Ridge

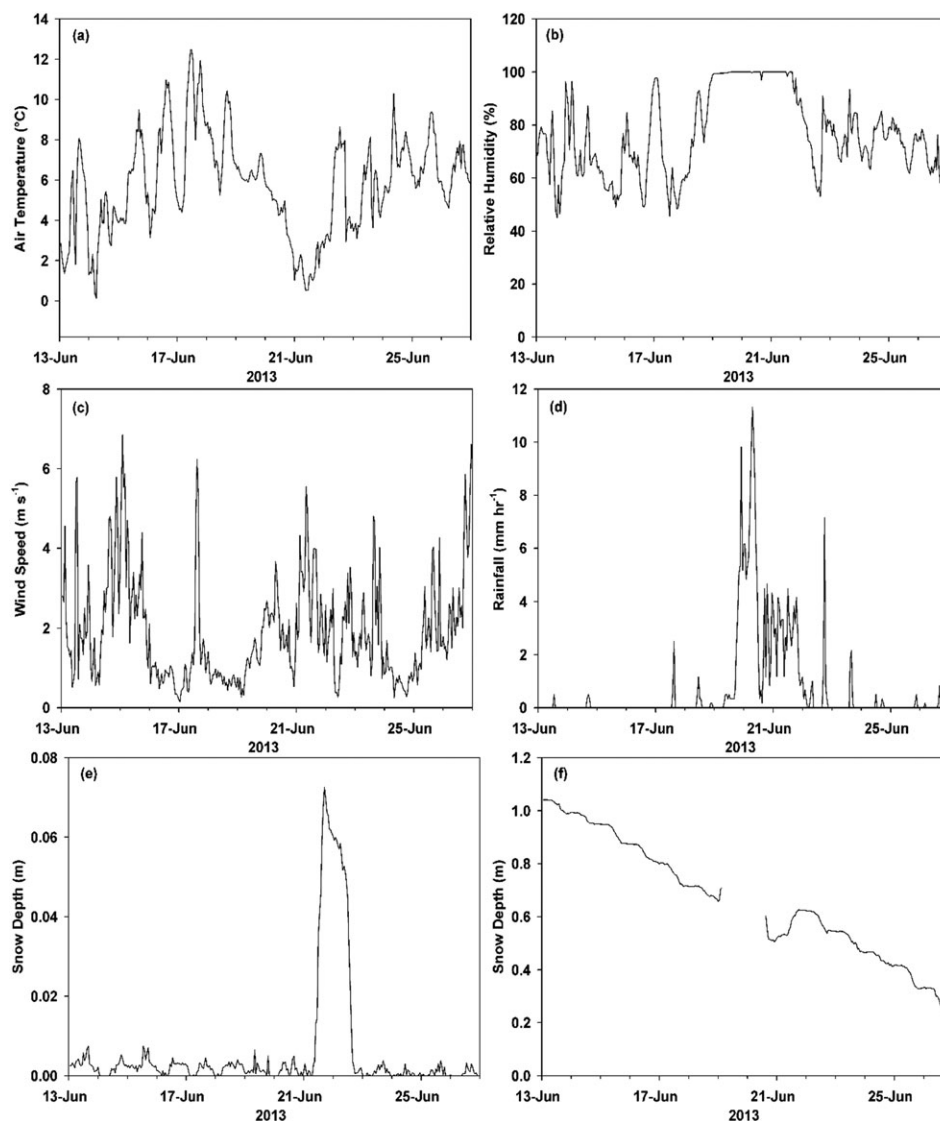


Figure 6. Meteorological conditions including (a) air temperature, (b) relative humidity, (c) wind speed, (d) hourly rainfall rate, (e) snow depth on the ground at Fisera Ridge meteorological station (2325 m) and (f) snow depth on the ground at Fisera South-face meteorological station before, during and after the flood period

was 201 mm, or  $16 \text{ mm day}^{-1}$ , and the average ablation for mostly open south-facing tundra sites on Fisera South-face that remained snow-covered was 252 mm or  $19 \text{ mm day}^{-1}$ .

#### Model testing and streamflow observations

Because of the uncertainty with discharge measurements during and after the flood and the lack of snow surveys during the flood, the UMCB model was tested in two ways: first, to establish its ability to simulate the multi-year snow regime on top of Fisera Ridge and on the Fisera south-face where monthly snow surveys of depth and density transects were available for several years, including the flood period in 2013, and second, to test its ability to simulate daily

stream discharge at the gauged outlet of Upper Marmot Creek up to the likely peak flow of the flood in 2013. The model was ran over a number of years with standard uncalibrated parameters (Fang *et al.*, 2013) so as not to bias its performance during a hydrometeorologically unique event from calibration to more typical snowmelt and rainfall events. The results are encouraging (Figure 7) as that model captures the seasonal cycle of snow accumulation and ablation with a root mean squared difference (RMSD) of 93 mm, a normalized RMSD of 0.43 and a mean bias of 0.17 for all snow surveys over 6 years. The model also simulates the flashy spring freshet dominated streamflow regime with a Nash–Sutcliffe efficiency of 0.54, a RMSD of  $0.036 \text{ m}^3 \text{ s}^{-1}$ , a normalized RMSD of 0.57 and a mean bias of  $-0.11$  over 5 years. The gauged



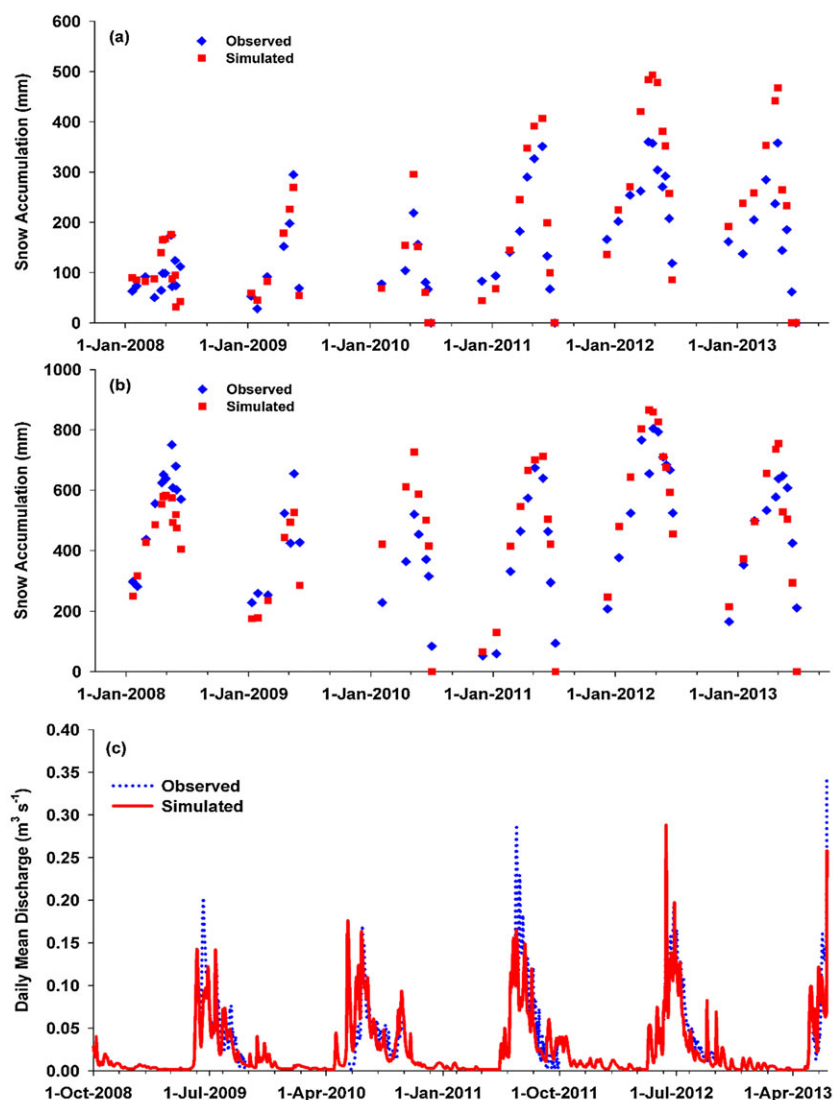


Figure 7. Modelled and measured snow water equivalent and streamflow. Snowpack snow water equivalent is shown for (a) Fisera Ridge and (b) Fisera South-face (lower half) for days when snow surveys were conducted, and streamflow is shown continuously as (c) daily discharge for Upper Marmot Creek

channel was disturbed by erosion and avulsion during the peak flow event, so the recorded peak flow during the event of  $0.35 \text{ m}^3 \text{ s}^{-1}$  is highly uncertain. Given uncertainties in driving meteorology, model structure, model parameters, initial conditions and evaluation data, the model provides reasonable simulations of SWE and streamflow that are considered sufficiently good to use to diagnose the ROS event.

#### *Modelled mass and energy budget for Fisera South-face snowdrift*

Figures 8 and 9 show hourly time series from 13–27 June 2013 and daily averages for periods before (13–18 June), during (19–22 June) and after (23–27 June) the flood for the external energy and mass budgets for the snowpack on Fisera South-face. The snowpack was

isothermal throughout the period of 13–27 June, so no internal energy is needed to be satisfied. The results show that before the flood, net shortwave radiation dominated the energy budget overall and during daylight, although sensible heat and net longwave radiation dominated the night-time energy budget and were a secondary source of overall energy for melt. The turbulent latent heat flux was predominately negative, removing energy from the snowpack via sublimation. Advective (rainfall) and ground heat terms were negligible. Similar conditions prevailed after the flood, with the difference that latent turbulent heat fluxes became positive, indicating condensation onto the snowpack as a result of more humid atmospheric conditions than before the flood. However, during the flood, the energy budget was quite different from pre- or post-flood fluxes. First, the total energy available for snowmelt dropped from an average of

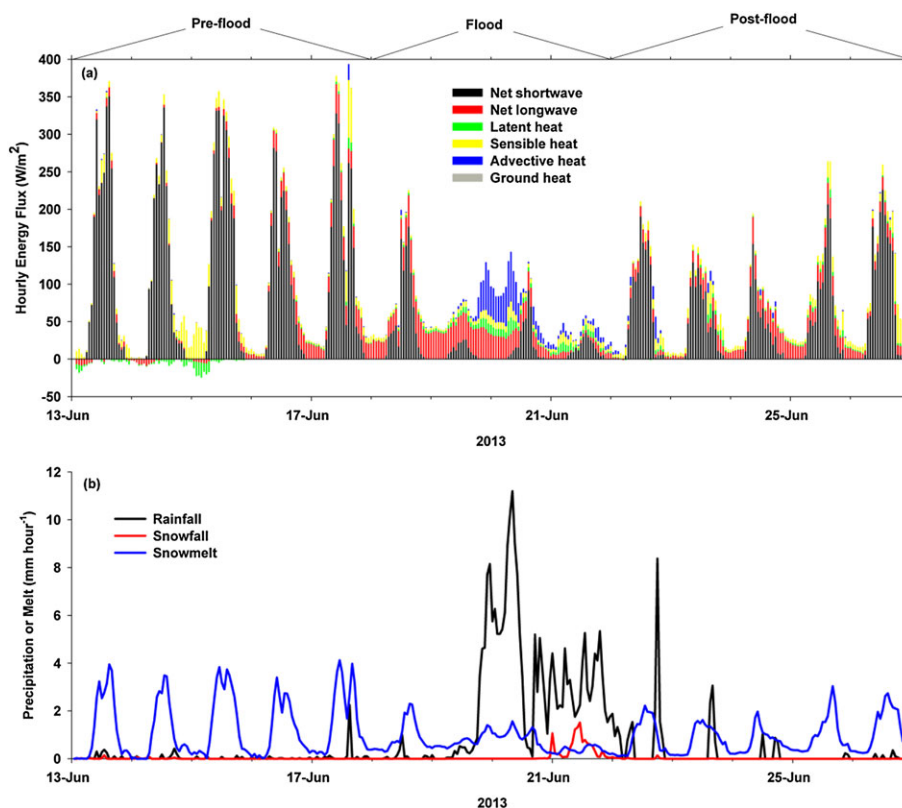


Figure 8. Simulated hourly (a) energy budget with terms aggregated to show net positive and net negative energy on an hourly basis and (b) modelled and measured hourly mass budget terms for Fisera Ridge South-face snowpack in June 2013. Positive energy fluxes are to the snowpack

$110 \text{ W m}^{-2}$  before the flood to  $64 \text{ W m}^{-2}$  during the flood and then rose to  $80 \text{ W m}^{-2}$  after the flood (Figure 9). The cloudy conditions during the flood caused a dramatic drop in net shortwave radiation from  $89$  to  $22 \text{ W m}^{-2}$  that was not compensated for by an increase in net longwave radiation from  $11$  to  $18 \text{ W m}^{-2}$ . Turbulent fluxes and advective heat from precipitation did not compensate for this either; although latent heat increased by  $6 \text{ W m}^{-2}$ , sensible heat declined by  $4 \text{ W m}^{-2}$ , and advected heat rose by only  $12 \text{ W m}^{-2}$  – the small turbulent and advected fluxes are a result of low wind speeds and dropping temperatures during the flood. Advected fluxes were only important on the 19th and 20th and by the 21st and 22nd when snowfall had occurred; advected and turbulent fluxes and net longwave radiation were very small contributions to snowmelt.

The snowpack mass budgets in Figures 8 and 9 show the strong impact of the flood precipitation. Pre-flood snowmelt peaked daily after peak insolation at about  $4 \text{ mm h}^{-1}$  with a daily average melt rate of  $28 \text{ mm day}^{-1}$ . A few short rainfall events on the 13th, 17th and 18th contributed on average only  $2 \text{ mm day}^{-1}$ , and snowmelt provided 93% of the water input to the ground surface. During the flood, snowmelt rates dropped by one third to  $17 \text{ mm day}^{-1}$  and were no longer associated with insolation; peak snowmelt rates dropped below 2 and

then below  $1 \text{ mm h}^{-1}$  as the atmosphere cooled during the flood. Rainfall averaged  $61 \text{ mm day}^{-1}$  during the flood with peak rates just under  $12 \text{ mm h}^{-1}$ , causing the snowmelt contribution of water input to the ground to drop to 22%. Snowfall rates during the flood remained below  $3 \text{ mm day}^{-1}$  and were negligible before and after the event. Post-flood snowmelt rates returned to an insolation-driven diel regime and increased to  $25 \text{ mm day}^{-1}$ , and 90% of water inputs supplied to the ground surface.

As a test of model outputs, the flood total calculations of 243 mm of rainfall and 12 mm water equivalent of snowfall are plausible given the 8 cm increase in snow depth during the flood – the wet, melting fresh snow is expected to be denser than typical densities of fresh dry snow (Pomeroy and Goodison, 1997). The event snowmelt of 68 mm water equivalent is plausible given 22 cm of snow depth decrease during the flood event, if the density of melting snow was about  $310 \text{ kg m}^{-3}$ . Snowmelt measured on the open section of Fisera South-face was 252 mm water equivalent, and that modelled between these early afternoon snow surveys on the 13th and 26th was 270 mm, a 7% overestimate. Given the uncertainties in snow survey measurements, driving meteorology, precipitation and model parameters, this is considered a good confirmation that the simulation

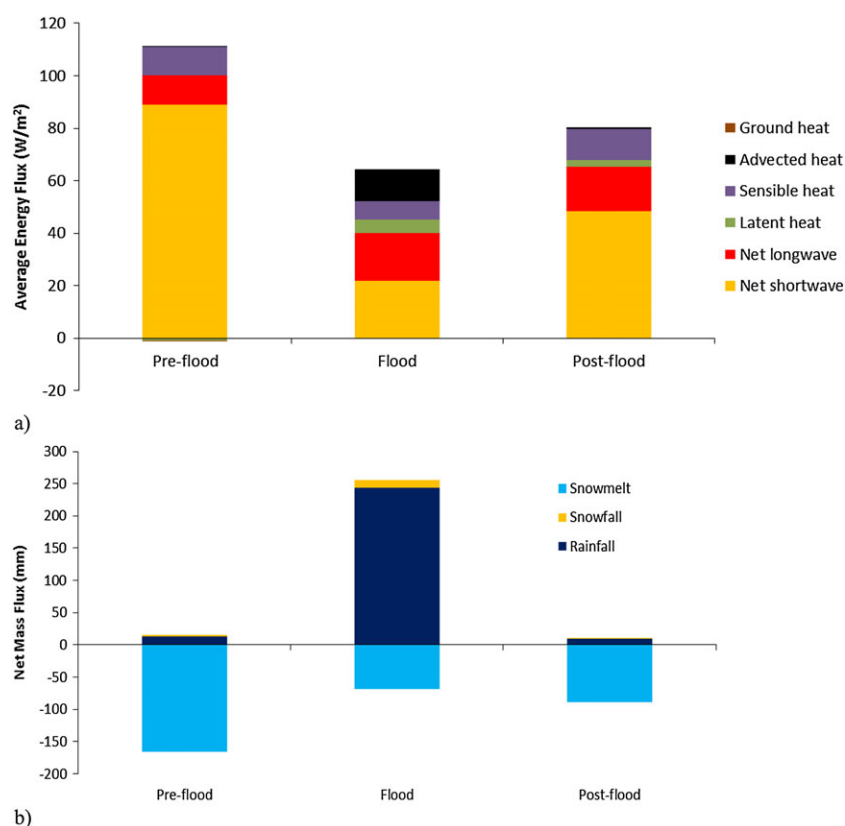


Figure 9. Pre-flood (13–18 June), flood (19–22 June) and post-flood (23–27 June) simulated (a) energy and (b) net mass fluxes to the Fisera South-face snowpack. The total energy flux to the snowpack in (a) is represented by the snowmelt flux in (b). Note energy fluxes are averages, and mass fluxes are totals over each of the three periods

was a plausible representation of snowmelt during the flood and in the period around the flood.

#### *Modelled mass and energy budget for Upper Marmot Creek Basin*

Figure 10 shows the daily net mass fluxes to UMCB and the streamflow discharge from the basin before, during and after the flood – mass balance closure over this period is 3 mm, suggesting that most storage from the flood had formed discharge by 2 July. Evaporation is a combination of evapotranspiration, evaporation from or condensation to snowpacks, evaporation of intercepted rainfall and sublimation of surface, blowing and intercepted snow. The term was dominated by evapotranspiration and evaporation of intercepted rainfall and was dampened during ROS by a very small depth of condensation to snowpacks. Sub-surface flow from the upper and lower soil layers was small (approximately  $4 \text{ mm day}^{-1}$ ) before the flood, increasing to  $23 \text{ mm day}^{-1}$  on 23 June and afterwards, slowly declining to values that remained twice those of the pre-flood period. Groundwater discharge that does not contribute to streamflow within UMCB responded slowly to the flood,

increasing from values just under to those just over  $4 \text{ mm day}^{-1}$ . Sub-surface storage of soil and ground water increased from 19 to 23 June with a peak increase of 23 mm on 22 June; storage subsequently decreased, contributing to streamflow from 24 June onwards. Whilst inputs of rainfall peaked on 20 June, when 113 mm of rainfall represented 97% of inputs to UMCB, streamflow discharge peaked on 21 June as a result of sub-surface storage of some rainfall on 20 June and an order of magnitude increase in snowmelt on 21 June. Rainfall inputs diminished rapidly after 20 June, down to 55 mm, and a 67% contribution to inputs on 21 June and 19 mm and 68% of inputs on 22 June. Snowmelt of  $3\text{--}5 \text{ mm day}^{-1}$  dominated inputs before 19 June and peaked on 21 June (27 mm). Snowmelt exceeded other inputs from 24 June onwards, ranging from 3 to  $8 \text{ mm day}^{-1}$ ; the increase over pre-flood rates was a result of increased snowcover after the flood.

A summary of pre-flood (12–18 June), flood (19–25 June) and post-flood (26 June–2 July) UMCB mass and energy fluxes is shown in Figure 11. Mass fluxes to all of the HRU and streamflow discharge from the basin are shown as mm averaged across MCRB and show the dramatic change from primarily snowmelt and rainfall

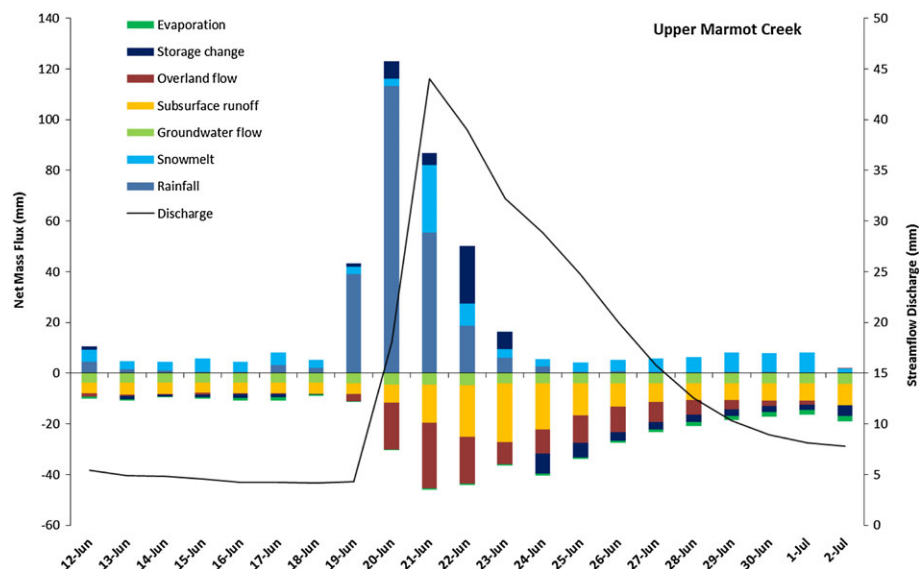


Figure 10. Daily net mass fluxes to all of the hydrological response units of UMCB, including streamflow discharge per unit area from the basin, after lagging, simulated for the period from 12 June to 2 July 2013

surface inputs before the flood, to rainfall and snowmelt inputs during the flood and to snowmelt and storage release inputs after the flood. Snowmelt (51 mm) was an additional 22% of input from rainfall (236 mm) during the flood, and snowmelt dominated surface inputs before (69%) and after (94%) the flood. As a result, total water delivery to the basin during the flood was 287 mm, 36 mm more than the precipitation during the event. Flow pathways also changed substantially, with groundwater and sub-surface flows dominating before the flood, sub-surface and overland flows during the flood and sub-surface and overland and groundwater flows after the flood. Streamflow discharge per unit area of the basin was closely matched to rainfall and snowmelt inputs before the flood, but during the flood, 191 mm of discharge was 67% of the rainfall and snowmelt inputs of 287 mm, and after the flood, discharge was double the snowmelt and rainfall inputs of 41 mm. This demonstrates the dynamic nature of storage in regulating streamflow response from this alpine basin.

The energy fluxes shown in Figure 11B are fluxes to the snow-covered area of UMCB expressed as fluxes per unit area of the basin – as a result, they are much smaller than and not directly comparable to fluxes per unit area of snowcover shown in Figure 9A for the Fisera South-face snowpack. The basin was only partially (15%) snow-covered at the beginning of the flood with snowpacks mainly on vegetated south-face slope HRUs. However, during the flood, snowfall resulted in snowcover expanding to the whole basin (100%), and this snowfall melted rapidly, resulting in a depletion of snow-covered area after the flood to levels similar to those before the flood. As a result, a ground heat flux to the fresh

snowpack of  $11 \text{ W m}^{-2}$  from previously exposed bare ground dominated basin-wide snowmelt energy during the flood. This increase in ground heat flux more than compensated for the halving of net shortwave radiation during the flood and was supplemented by small but positive latent, sensible and advected heat fluxes totalling  $5 \text{ W m}^{-2}$ . Turbulent and advected fluxes were small because of the low wind speeds and very cool temperatures that prevailed after the snowcover increased on 21 June. Basin total melt energy rose 52% from  $17 \text{ W m}^{-2}$  before the flood to  $26 \text{ W m}^{-2}$  during the flood and remained high ( $22 \text{ W m}^{-2}$ ) as snowcover declined after the flood. This substantial increase is largely a result of the increase in snow-covered area and ground heat flux contribution.

## DISCUSSION

The early summer June 2013 flood in the alpine sub-basin of Marmot Creek was distinctive in many ways from most documented mid-winter ROS floods. Whilst it started with warm air temperatures following a period of temperate, sunny and dry early-summer weather, air temperatures cooled off by  $7^\circ\text{C}$  during the event, such that rainfall turned to snowfall on the 21st. This cooling both dampened heat fluxes to snow from incoming longwave radiation, advected heat in precipitation, turbulent sensible heat and turbulent latent heat and increased the snow-covered area and SWE available to drive snowmelt. Wind speeds remained low during the ROS event. As a result, although snowmelt energy to existing snowpacks declined during the ROS as a result of the reduction in net shortwave

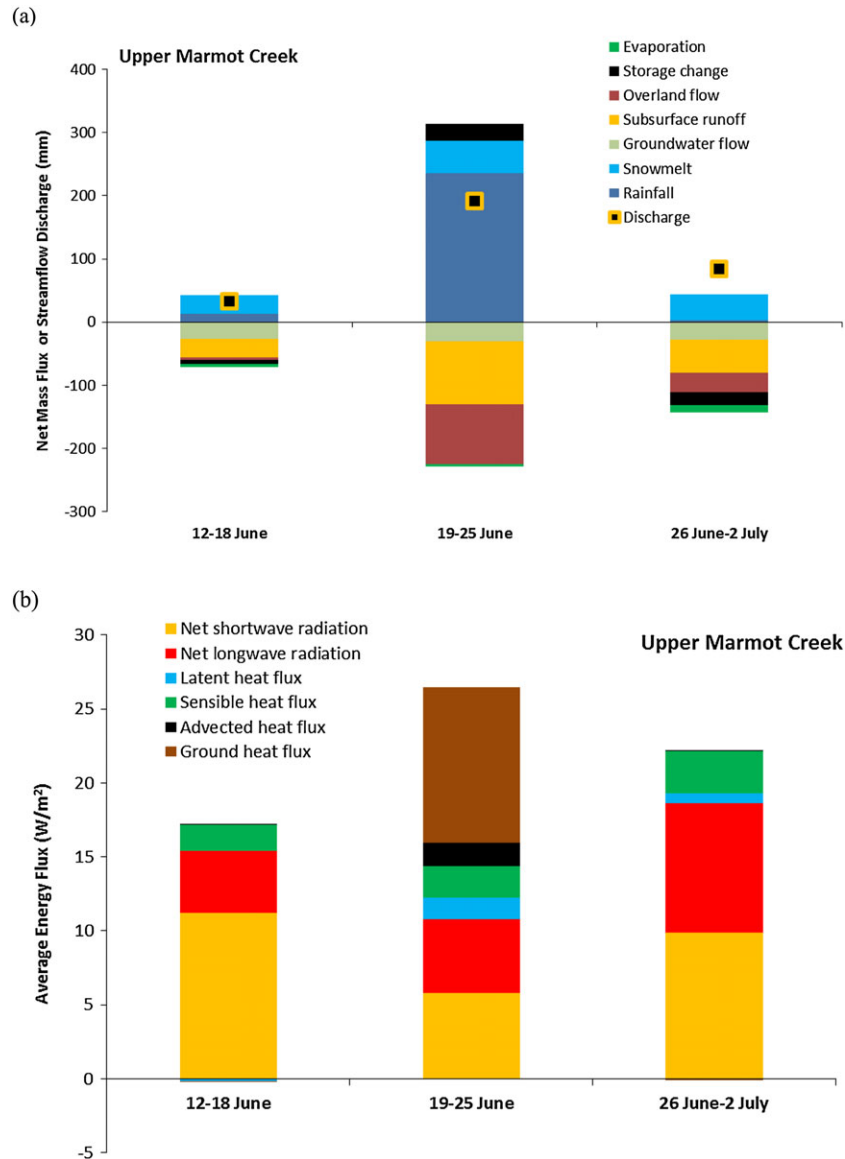


Figure 11. Pre-flood, flood and post-flood (a) net mass fluxes and streamflow discharge for Upper Marmot Creek Basin and (b) average energy fluxes to the snow-covered area of the basin

radiation exceeding the net increases in advected heat, longwave radiation and the turbulent heat fluxes, the areally averaged snowmelt energy to the basin increased as a result of the increase in snow-covered area and ground heat fluxes from newly snow-covered warm ground into the snowpack. This differs substantially from the classic mid-winter ROS of substantially increased sensible and latent heat fluxes along with advected energy driving more rapid snowmelt described by Marks *et al.* (1998, 2001) and Mazurkiewicz *et al.* (2008). So, although snowmelt rates of existing snowpacks dropped by one third during the flood, snowmelt from the basin increased by almost one half, and snowmelt formed an appreciable ( $>1/5$ th) contribution to water inputs to the alpine basin during the flood. This type of summer ROS behaviour has not been described before

and may be characteristic of the late-spring and early-summer floods in the Canadian Rockies that occurred frequently in the late 19th and early 20th centuries. (Whitfield and Pomeroy, 2016). The snowmelt processes described here are likely typical of summer runoff events in Canadian Rockies mountain headwaters where the persistence of snowpacks into July at high elevations coincides with the annual rainy season (Pomeroy *et al.*, 2016).

The change in flow pathways as a result of the large precipitation volumes in this event is also instructive. Marmot Creek streamflow generation is normally dominated by sub-surface flow (Harlan, 1969; Pomeroy *et al.*, 2012; Fang *et al.*, 2013), but during the flood, seldom-activated overland flow processes became equal to sub-surface flow and help to explain the remarkable



celerity of the streamflow response recorded in the region during this event (Pomeroy *et al.*, 2016; Whitfield and Pomeroy, 2016). The implication of changing flow pathways as the flood peaked and the changing sources from rainfall to snowmelt runoff as the flood persisted is that a hydrological model chosen from or calibrated on the non-flood conditions that have persisted because Marmot Creek was first gauged in 1961 might not have an adequate structure or calibrations to predict the 2013 flood with accuracy. The deficiencies of calibrated conceptual models would have remained hidden until an attempt at flood simulation of a complex ROS event such as in 2013. Yet Whitfield and Pomeroy (2016) show that events like 2013 are responsible for most notable peak flow events in the region. Because the model used in this study has a strong physical basis, including snow redistribution by wind, psychrometric precipitation phase, energy budget snowmelt and a full range of surface and sub-surface runoff generation and streamflow discharge forming processes, and was parameterized using measurements of physically identifiable variables rather than by attempting to mimic the hydrograph, it is felt to be more likely that the hydrograph simulations are correct for the right reasons.

A critical feature of the modelling was that a model must be able to redistribute alpine snow by blowing snow to form late-lying snowpacks in the first place. Winstral and Marks (2002) and Musselman *et al.* (2015) have shown that correct simulation of windflow and over-winter wind redistribution and sublimation of snow is essential to modelling snowmelt dynamics in cold windy alpine environments such as UMCB. Large late-lying alpine snowdrifts on the Fisera South-face near treelines and in topographic breaks were an important feature in Marmot Creek that made this ROS flood possible. The importance of condensation and advected rain energy during the event in the energy budget indicates that less physically based simulation techniques such as the temperature-index approach that do not consider transient energy and mass fluxes such as latent heat and advected energy and are calibrated on non-rain snowmelt events would be highly uncertain during this type of ROS event.

## CONCLUSIONS

A large rainfall event at high elevations fell on a substantial mountain snowpack in the Alberta June 2013 flood. The rainfall terminated as it turned to snowfall on day three of the flood (21 June). It was possible to successfully model snowpack dynamics and streamflow using a physically based CRHM in a small alpine sub-basin without calibration of parameters from streamflow. Using the model to diagnose the event, it was

found that snowmelt energy and melt rates over a late lying south-facing slope snow drift snowpack declined during the flood compared with pre- and post-flood periods as a result of reduced shortwave radiation. During the flood, net longwave radiation, sensible and latent heat and advected energy only partly compensated for reduced net shortwave radiation fluxes as a result of cool air temperatures and low wind speeds. However, at the basin scale, an increase in snow-covered area as a result of snowfall at the end of the flood provided a snowpack which melted quickly – partly as a result of a large ground heat flux. Whilst rainfall–runoff dominated the flood runoff generation, snowmelt became progressively more important as the flood progressed. Snowmelt totals over the basin during the flood were larger by almost half of those in periods just before or after, and snowmelt contributed just over one fifth of basin discharge during the flood. Streamflow generation mechanisms were evenly divided between subsurface flow and overland flow during the flood; however, overland flow was negligible before the flood and only one third of runoff after the flood. Overland flow resulted in rapid generation of the flow peak, but flow celerities were tempered by overland flow through the snowpack and organic material above the soil. Subsurface storage was recharged during the flood and discharged afterwards, causing 1 week of higher than normal streamflow after the flood.

The ROS flood event was distinctive in that it was predicated on over-winter wind redistribution of snow into deep alpine and sub-alpine snowdrifts that persisted into summer, that the energy sources for snowmelt shifted from primarily solar radiation before and after the event to a combination of fluxes of longwave radiation, turbulent heat, ground heat and advected heat from rainfall during the event, and that runoff pathways shifted from sub-surface before the event to an even mix of overland flow and sub-surface flow during and shortly after the event. A unique aspect to this event was that whilst snowmelt rates for existing snowpacks declined during the event compared with before or after, the rapid, ground heat-driven melt of fresh snowfall near the end increased snowmelt contributions to runoff over the alpine basin such that snowmelt was a major contribution to flood streamflow discharge. Although not previously described in the scientific literature, this type of ROS event may be characteristic of exceptionally large, historical, late-spring and early-summer flood events in the Canadian Rockies and other similar cold region mountain headwaters. The dramatic changes in melt rates, snowmelt contributing areas and runoff celerities during this event suggest that conceptual approaches to hydrological modelling that are conditioned or calibrated to non-flood conditions would introduce great uncertainty to simulation, and that some physical calculations that are seldom used in day-to-day

hydrological simulations can be crucial to simulating the hydrological behaviour of extreme events.

#### ACKNOWLEDGEMENTS

The authors wish to acknowledge funding from Alberta departments of Agriculture and Forestry and Environment and Parks, the Natural Sciences and Engineering Research Council of Canada (NSERC) through its Discovery and Research Tools and Instruments Grants, the Canadian Foundation for Innovation, the NSERC Changing Cold Regions Network, Canada Research Chairs programme, the Canada Excellence Research Chair in Water Security, the Canadian Foundation for Climate and Atmospheric Sciences and the USDA Agricultural Research Service and logistical assistance from Nakiska Ski Resort and the Biogeoscience Institute of the University of Calgary.

#### REFERENCES

- Beke GJ. 1969. Soils of three experimental watersheds in Alberta and their hydrological significance. Unpublished Ph.D. Thesis, Department of Soil Science, University of Alberta, Edmonton, 456.
- Brooks RH, Corey AT. 1964. *Hydraulic Properties of Porous Media*, Hydrology Paper 3, Colorado State University: Fort Collins, Colorado; 27.
- Brooks RH, Corey AT. 1966. Properties of porous media affecting fluid flow. *Proceedings of the American Society of Civil Engineers, Irrigation and Drainage Division* **92**(IR2): 61–88.
- Buttle J, Allen D, Caissie D, Davison B, Hayashi M, Peters D, Pomeroy JW, Simonovic S, St-Hilaire A, Whitfield P. 2016. Flood processes in Canada: regional and special aspects. *Canadian Water Resources Journal* **41**(1–2): 7–30. DOI:10.1080/07011784.2015.1131629.
- Clark MP, Nijssen B, Lundquist J, Kavetski D, Rupp DE, Gutmann E, Wood A, Brekke L, Arnold JR, Gochis D, Rasmussen R. 2015a. A unified approach to hydrologic modeling: Part 1. Modeling concept. *Water Resources Research* **51**: 2498–2514. DOI:10.1002/2015WR017198
- Clark MP, Nijssen B, Lundquist J, Kavetski D, Rupp DE, Gutmann E, Wood A, Gochis D, Rasmussen R, Tarboton D, Mahat V, Flerchinger G, Marks D. 2015b. A unified approach to hydrologic modeling: part 2. Model implementation and case studies. *Water Resources Research* **51**: 2515–2542. DOI:10.1002/2015WR017200
- Colbeck SC. 1972. A theory for water percolation in snow. *Journal of Glaciology* **11**: 369–385.
- Colbeck SC. 1975. A theory for water flow through a layered snowpack. *Water Resources Research* **11**: 261–266.
- DeBeer CM, Pomeroy JW. 2010. Simulation of the snowmelt runoff contributing area in a small alpine basin. *Hydrology and Earth System Sciences* **14**: 1205–1219. DOI:10.5194/hess-14-1205-2010
- Dumanski S, Pomeroy JW, Westbrook CJ. 2015. Hydrological regime changes in a Canadian Prairie basin. *Hydrological Processes* **29**: 3893–3904. DOI:10.1002/hyp.10567
- Ellis CR, Pomeroy JW. 2007. Estimating sub-canopy shortwave irradiance to melting snow on mountain slopes. *Hydrological Processes* **21**: 2581–2597. DOI:10.1002/hyp.6794
- Ellis CR, Pomeroy JW, Brown T, MacDonald J. 2010. Simulation of snow accumulation and melt in needleleaf forest environments. *Hydrology and Earth System Sciences* **14**: 925–940. DOI:10.5194/hess-14-925-2010
- Ellis CR, Pomeroy JW, Essery RLH, Link TE. 2011. Effects of needleleaf forest cover on radiation and snowmelt dynamics in the Canadian Rocky Mountains. *Canadian Journal of Forest Research* **41**: 608–620. DOI:10.1139/X10-227
- Ellis CR, Pomeroy JW, Link TE. 2013. Modeling increases in snowmelt yield and desynchronization resulting from forest gap thinning treatments in a northern mountain catchment. *Water Resources Research* **49**: 936–949. DOI:10.1002/wrcr.20089
- Fang X, Pomeroy J. 2016. Impact of antecedent conditions on simulations of a flood in a mountain headwater basin. *Hydrological Processes* this issue DOI:10.1002/hyp.10910.
- Fang X, Pomeroy JW, Ellis CR, MacDonald MK, DeBeer CM, Brown T. 2013. Multi-variable evaluation of hydrological model predictions for a headwater basin in the Canadian Rocky Mountains. *Hydrology and Earth System Sciences* **17**: 1635–1659. DOI:10.5194/hess-17-1635-2013
- Garvelmann J, Pohl S, Weiler M. 2015. Spatio-temporal controls of snowmelt and runoff generation during rain-on-snow events in a mid-latitude mountain catchment. *Hydrological Processes* **29**: 3649–3664. DOI:10.1002/hyp.10460
- Harder P, Pomeroy JW. 2013. Estimating precipitation phase using a psychrometric energy balance method. *Hydrological Processes* **27**: 1901–1914. DOI:10.1002/hyp.9799
- Harder P, Pomeroy JW. 2014. Hydrological model uncertainty due to precipitation-phase partitioning methods. *Hydrological Processes* **28**: 4311–4327. DOI:10.1002/hyp.10214
- Harlan RL. 1969. Soil–water freezing, snow accumulation and ablation in Marmot Creek Experimental Watershed, Alberta, Canada. Proceedings of the 37th Western Snow Conference, 15–17 April 1969, Salt Lake City, Utah, 29–33.
- Harr RD. 1981. Some characteristics and consequences of snowmelt during rainfall in western Oregon. *Journal of Hydrology* **53**: 277–304.
- Hopkinson C, Pomeroy JW, DeBeer C, Ellis C, Anderson A. 2012. Relationships between snowpack depth and primary LiDAR point cloud derivatives in a mountainous environment. Proceedings of the Remote Sensing and Hydrology Symposium, IAHS Publication No. 352, 354–358.
- Jeffrey WW. 1965. Experimental watersheds in the Rocky Mountains, Alberta, Canada. Proceedings of the Symposium on Representative and Experimental Areas, IAHS Publication No. 66, 502–521.
- Keith DM, Johnson EA, Valeo C. 2010. A hillslope forest floor (duff) water budget and the transition to local control. *Hydrological Processes* **24**: 2738–2751. DOI:10.1002/hyp.7697
- Liu A, Mooney C, Szeto K, Thériault JM, Kochubajda B, Stewart RE, Boodoo S, Goodson R, Li Y, Pomeroy J. 2016. The June 2013 Alberta catastrophic flood event: part 1 — climatological aspects and hydrometeorological features. *Hydrological Processes* this issue DOI:10.1002/hyp.10906.
- MacDonald MK, Pomeroy JW, Pietroniro A. 2010. On the importance of sublimation to an alpine snow mass balance in the Canadian Rocky Mountains. *Hydrology and Earth System Sciences* **14**: 1401–1415. DOI:10.5194/hess-14-1401-2010
- Marks D, Kimball J, Tingey D, Link T. 1998. The sensitivity of snowmelt processes to climate conditions and forest cover during rain-on-snow: a case study of the 1996 Pacific Northwest flood. *Hydrological Processes* **12**: 1569–1587.
- Marks D, Link T, Winstral A, Garen D. 2001. Simulating snowmelt processes during rain-on-snow over a semi-arid mountain basin. *Annals of Glaciology* **32**: 195–202. DOI:10.3189/172756401781819751
- Mazurkiewicz AB, Callery DG, McDonnell JJ. 2008. Assessing the controls of the snow energy balance and water available for runoff in a rain-on-snow environment. *Journal of Hydrology* **354**: 1–14.
- McCabe GJ, Clark MP, Hay LE. 2007. Rain-on-snow events in the western United States. *Bulletin of the American Meteorological Society* **88**: 319–328.
- McGurk BJ, Kattelmann RC. 1986. Water flow rates, porosity, and permeability in snowpacks in the Central Sierra Nevada. In *Cold Regions Hydrology Symposium*, Kane DL (ed), Fairbanks, Alaska. Proceedings. American Water Resources Association: Bethesda, MD; 359–366.
- Musselman KN, Pomeroy JW, Essery RLH, Leroux N. 2015. Impact of windflow calculations on simulations of alpine snow accumulation, redistribution and ablation. *Hydrological Processes* **29**: 3983–3999.
- Pomeroy JW, Goodison BE. 1997. Winter and snow. In *The Surface Climates of Canada*, Bailey WG, Oke TR, Rouse WR (eds). McGill-Queen's University Press: Montreal & Kingston; 68–100.
- Pomeroy JW, Li L. 2000. Prairie and Arctic areal snow cover mass balance using a blowing snow model. *Journal of Geophysical Research* **105**: 26619–26634.
- Pomeroy JW, Gray DM, Brown T, Hedstrom NR, Quinton W, Granger RJ, Carey S. 2007. The Cold Regions Hydrological model, a platform

- for basing process representation and model structure on physical evidence. *Hydrological Processes* **21**: 2650–2667. DOI:10.1002/hyp.6787
- Pomeroy JW, Marks D, Link T, Ellis C, Hardy J, Rowlands A, Granger R. 2009. The impact of coniferous forest temperature on incoming longwave radiation to melting snow. *Hydrological Processes* **23**: 2513–2525. DOI:10.1002/hyp.7325
- Pomeroy JW, Fang X, Ellis C. 2012. Sensitivity of snowmelt hydrology in Marmot Creek, Alberta, to forest cover disturbance. *Hydrological Processes* **26**: 1892–1905. DOI:10.1002/hyp.9248
- Pomeroy JW, Stewart RE, Whitfield PH. 2016. The 2013 flood event in the Bow and Oldman River basins: causes, assessment and damages. *Canadian Water Resources Journal* **41**(1-2): 105–117. DOI:10.1080/07011784.2015.1089190.
- Pradhanang SM, Frei A, Zion M, Schneiderman EM, Steenhuis TS, Pierson D. 2013. Rain-on-snow runoff events in New York. *Hydrological Processes* **27**: 3035–3049. DOI:10.1002/hyp.9864
- Rasouli K, Pomeroy JW, Marks DG. 2015. Snowpack sensitivity to perturbed climate in a cool mid-latitude mountain catchment. *Hydrological Processes* **29**: 3925–3940. DOI:10.1002/hyp.10587
- Shimizu H. 1970. Air permeability of deposited snow. *Contributions from the Institute of Low Temperature Science, Series A* **22**: 1–32.
- Sicart JE, Pomeroy JW, Essery RLH, Bewley D. 2006. Incoming longwave radiation to melting snow: observations, sensitivity and estimation in northern environments. *Hydrological Processes* **20**: 3697–3708. DOI:10.1002/hyp.6383
- Singh P, Kumar N. 1997. Effect of orography on precipitation in the western Himalayan region. *Journal of Hydrology* **199**: 183–206.
- Singh P, Spitzbart G, Hübl H, Weinmeister HW. 1997. Hydrological response of snowpack under rain-on-snow events: a field study. *Journal of Hydrology* **202**: 1–20.
- Stadnyk T, Dow K, Wazney L, Blais E. 2016. The 2011 flood event in the Red River Basin: causes, assessment and damages. *Canadian Water Resources Journal* **41**(1-2): 65–73. DOI:10.1080/07011784.2015.1008048.
- Storr D. 1967. Precipitation variation in a small forested watershed. Proceedings of the 35th Annual Western Snow Conference, 18–20 April 1967, Boise, Idaho; 11–17.
- Sui J, Koehler G. 2001. Rain-on-snow induced flood events in Southern Germany. *Journal of Hydrology* **252**: 205–220.
- Swanson RH. 1998. Forest hydrology issues for the 21st century: a consultant's viewpoint. *Journal of the American Water Resources Association* **34**(4): 755–763.
- Walmsley JL, Taylor PA, Salmon JR. 1989. Simple guidelines for estimating wind speed variations due to small-scale topographic features — an update. *Climatological Bulletin* **23**: 3–14.
- Walter MT, Brooks ES, McCool DK, King LG, Molnau M, Boll J. 2005. Process-based snowmelt modelling: does it require more input data than temperature-index modelling? *Journal of Hydrology* **300**: 65–75.
- Wankiewicz A. 1979. A review of water movement in snow. In *Proceedings of a Meeting on Modelling of Snow Cover Runoff*, Colbeck SC, Ray M (eds). Cold Regions Research and Engineering Laboratory: Hanover, New Hampshire; 222–252.
- Wayand N, Lundquist JD, Clark MP. 2015. How important is snow during rain-on-snow floods over the Western U.S. Mountains? *Water Resources Research* DOI:10.1002/2014WR016576, In Press
- Whitfield PH, Pomeroy JW. 2016. Changes to flood peaks of a mountain river: implications for analysis of the 2013 flood in the Upper Bow River, Canada. *Hydrological Processes* this issue
- Winstral A, Marks D. 2002. Simulating wind fields and snow redistribution using terrain-based parameters to model snow accumulation and melt over a semi-arid mountain catchment. *Hydrological Processes* **16**: 3585–3603.
- Ye H, Yang D, Robinson D. 2008. Winter rain on snow and its association with air temperature in northern Eurasia. *Hydrological Processes* **22**: 2728–2736. DOI:10.1002/hyp.7094